One-dimensional topological superconductivity at the edges of twisted bilayer graphene nanoribbons

Zhen-Hua Wang,[1,2,3] Fuming Xu,[1] Lin Li,[4,2] Rong Lü,[5,6] Bin Wang,[1,7,*] and Wei-Qiang Chen[2,7,†]

[1]*Shenzhen Key Laboratory of Advanced Thin Films and Applications, College of Physics and Optoelectronic Engineering, Shenzhen University, Shenzhen 518060, China*

[2]*Shenzhen Institute for Quantum Science and Engineering and Department of Physics, Southern University of Science and Technology, Shenzhen 518055, China*

[3]*Beijing Computational Science Research Center, Beijing 100193, China*

[4]*College of Physics and Electronic Engineering and Center for Computational Sciences, Sichuan Normal University, Chengdu 610068, China*

[5]*Department of Physics, Tsinghua University, Beijing 100084, China*

[6]*Collaborative Innovation Center of Quantum Matter, Beijing 100084, China*

[7]*Center for Quantum Computing, Peng Cheng Laboratory, Shenzhen 518055, China*

(Received 27 March 2019; revised manuscript received 14 August 2019; published 27 September 2019)

Twisted bilayer graphene is one of the simplest van der Waals structures, and its inhomogeneous interlayer coupling can induce rich electronic properties. In twisted bilayer graphene nanoribbons (tBLGNRs), the interlayer coupling strengths are different for two ribbon edges due to the inhomogeneous bonding, which splits the edge states into two individuals in energy. The lower-energy state, localizing at the ribbon edge with the stronger interlayer coupling, is a good candidate to generate one-dimensional (1D) topological superconductivity in the presence of Rashba spin-orbit coupling, Zeeman field, and *s*-wave superconductivity. Majorana zero modes (MZMs) are found to be localized at both ends of this edge. The topological invariants of the system are explored by evaluating the Berry phase for infinite-length ribbons and Majorana polarization for quasi-1D ribbons, giving the same topological phase diagram. More importantly, by adjusting interlayer dislocation and uniaxial strain of tBLGNRs across the critical values, the lower-energy edge changes and 1D topological superconductivity can "jump" from one ribbon edge to the other one. Finally, by applying a gate voltage bias between bilayers or changing the interlayer distance, a MZM can transfer along the ribbon edge. The tBLGNRs provide an alternative platform to study 1D topological superconductivity and MZMs.

DOI: 10.1103/PhysRevB.100.094531

I. INTRODUCTION

The Majorana fermion has become one of the most important fundamental quasiparticles of condensed-matter physics. Various platforms have been proposed to realize such an exotic particle. Signatures of Majorana fermions have already been found in semiconducting nanowires with strong spin-orbit coupling (SOC) in proximity to a superconductor [1–6], at the end of atomic iron chains on the surface of a superconductor [7], and in the hybrid system of a quantum anomalous Hall insulator coupled with a superconductor as one-dimensional (1D) chiral modes [8]. Majorana zero modes (MZMs) obey non-Abelian statistics [9,10] and are seen as promising building blocks to realize decoherence-free topological quantum computation [11,12]. The underlying condensed-matter support of the bounded Majorana zero modes will certainly play a key role, dictating how easily Majorana fermions can be braided or manipulated in general. Twisted bilayer graphene (tBLG) with its high tunability and rich properties is also a tempting platform.

During the last few years, tBLG has attracted much attention [13–20]. Apart from bilayer graphene's unconventional behavior, e.g., band-gap opening [21,22], and unique Raman [23,24] and infrared optical spectra [25,26], it has received new electronic properties by twist. Due to the moiré pattern, the wave function of Dirac electrons becomes localized, and this localization is maximum in the limit of the small twist angle between the two layers [27,28]. At the first magic angle $\theta \approx 1.1^\circ$, Mott-insulating behavior [29] and unconventional superconductivity [30] have been observed in tBLG. By varying the interlayer spacing with hydrostatic pressure, the capability to induce superconductivity at a twist angle larger than 1.1° is also established [18,31]. In twisted bilayer graphene nanoribbons (tBLGNRs), the interplay of edge and spatially inhomogeneous interlayer coupling makes the edge states from *AB*- and *AA*-stacked regions split in energy [32], and the low-energy transport properties are governed by the edge states with *AB* stacking [33]. It is also interesting to study the topological superconductivity based on the edge states of the tBLGNRs.

The topological superconductivity in single-layer graphene nanoribbons (GNRs) has been achieved in several proposals. The SOC in graphene can be enhanced by several orders by three different methods: proximity to high-SOC transition-metal dichalcogenides [34,35], via graphene hydrogenation [36], and a spatially varying magnetic field [37], and therefore the Majorana zero modes could be obtained based on the standard ingredients with Rashba SOC, Zeeman field, and

*binwang@szu.edu.cn
†chenwq@sustech.edu.cn

s-wave superconductivity [37–40]. Meanwhile, the interaction-induced magnetic ordering of graphene's zero Landau level gives rise to topological superconductivity when the graphene edge is in proximity to a conventional superconductor [41]. In proximity to a superconductor, the ends of effective antiferromagnetic Heisenberg spin-1/2 chains introduced by a 7/9-armchair GNR superlattice with robust spin are predicted to host Majorana fermion states [42]. As depositing bilayer graphene on a transition-metal dichalcogenide (TMD) monolayer, topological nontrivial phases can also be induced [43]. In graphenelike materials, such as TMD [44–46], the zigzag edge is also used to support robust topological Majorana bound states at the edge ends, although the two-dimensional bulk itself is nontopological.

In the present work, we predict that 1D topological superconductivity can be achieved at the edge of tBLGNRs and the MZMs appear at both ends of this edge in the presence of the Rashba spin-orbit coupling, Zeeman field, and *s*-wave superconductivity. The topological invariant is calculated to characterize the infinite ribbon, and the Majorana polarization is evaluated for the quasi-1D ribbons, which give the same phase diagram. By changing the interlayer dislocation or uniaxial strain, the lower-energy edge changes and the 1D topological superconductivity can "jump" from one ribbon edge to the other one. Moreover, the MZMs can be driven to transfer along the 1D ribbon edge by changing the gate voltage bias between bilayers and the interlayer distance.

The paper is organized as follows: In Sec. II, we introduce the minimum model used to describe the tBLGNRs in the Majorana physics regime. The verification of topological phase transition for an infinite ribbon and fully open system is also included. In Sec. III, we calculate the MZMs, the multiband Berry phase as the topological invariant to characterize the infinite ribbon, and the Majorana polarization for fully open ribbons. In Sec. IV, the "jump" of MZMs between two ribbon edges and the transfer of a MZM along the 1D ribbon edge are presented. In Secs. V and VI, the experimental realization of our model and concluding remarks are given, respectively.

II. MODEL

Figure 1(a) shows a schematic structure of *AB*-stacked bilayer graphene, where $\mathbf{a_1}$ and $\mathbf{a_2}$ are the same primitive vectors of the layer $l = 1, 2$. The tBLG can be generated by rotating the top and the bottom layers of the *AB*-stacked bilayer around a common *B* site by $-\varphi/2$ and $+\varphi/2$, respectively [32]. The primitive lattice vectors $\mathbf{L_1}$ and $\mathbf{L_2}$ on the twisted two layers are defined as [15,47,48] $\mathbf{L_1} = m\mathbf{a_1^{(1)}} + n\mathbf{a_2^{(1)}} = n\mathbf{a_1^{(2)}} + m\mathbf{a_2^{(2)}}$, where m, n are integers and related to the rotation angle φ. $\mathbf{L_2}$ is obtained by rotating $\mathbf{L_1}$ with 60° along the counterclockwise direction, and thus tBLG is specified by a single pair of integers (m, n). The rotation angle φ is related to (m, n) by

$$\cos\varphi = \frac{1}{2}\frac{m^2 + n^2 + 4mn}{m^2 + n^2 + mn}, \tag{1}$$

and the commensurate unit cell contains $N = 4(m^2 + n^2 + mn)$ atoms. Figure 1(b) shows the atomic structures of (1,2) tBLG with corresponding rotation angle $\varphi = 21.8°$, where the blue parallelogram in the lower right corner indicates its primitive cell.

In principle, a tBLGNR can be generated by repeating the unit cell of tBLG along the directions of $\mathbf{L_1}$ or $\mathbf{L_2}$, i.e., $N_x\mathbf{L_1} + N_y\mathbf{L_2}$. For the (1,2) tBLGNR of concern in the present work,

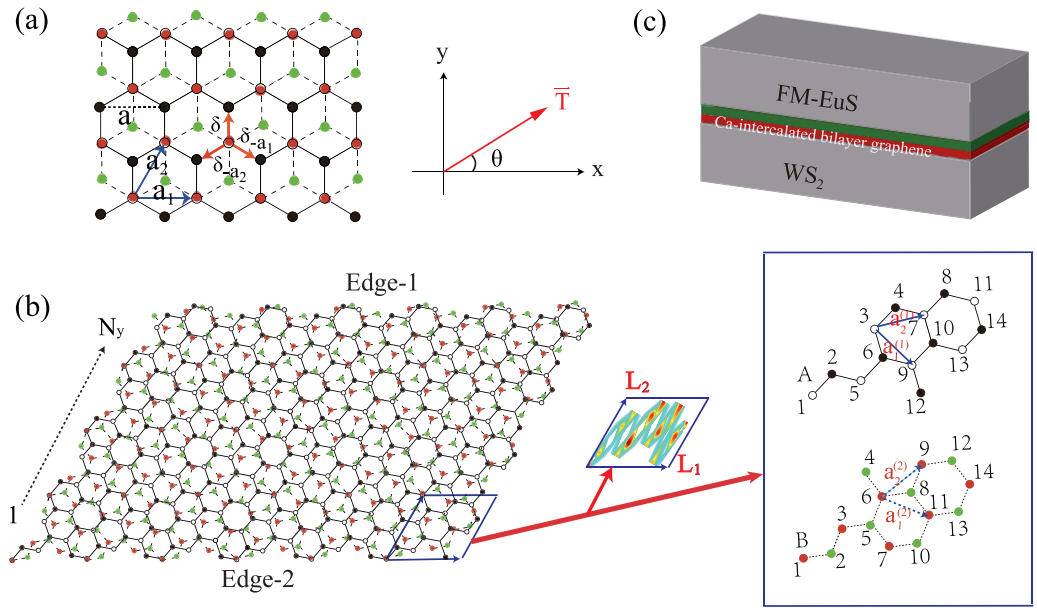

FIG. 1. (a) Lattice structure of *AB*-stacked bilayer graphene. Solid and dashed lines represent lattices of top and bottom layers, respectively. $\boldsymbol{\delta}$ are the vectors connecting the nearest-neighbor atoms, $\mathbf{a_1}$ and $\mathbf{a_2}$ are the primitive vectors, and θ is the direction of applied tension $\mathbf{T}$. (b) Lattice structure of (1,2) tBLGNR with $N_y = 4$ and rotation angle $\varphi = 21.8°$ based on $\mathbf{a_1}^{(l)}$ and $\mathbf{a_2}^{(l)}$. The blue parallelogram in the lower right corner defined by $\mathbf{L_1}$ and $\mathbf{L_2}$ indicates a unit cell of (1,2) tBLG. Inset of (b): The atomic structure and the interlayer coupling distribution in the unit cell. The interlayer coupling is stronger in edge 1. (c) Configuration of experimental proposals: tBLGNR sandwiched between WS_2 and ferromagnetic insulator EuS, decorated with alkali-metal atoms Ca or Li.

the length is along the $\mathbf{L_1}$ direction and N_x tends to infinity, while the width is along the $\mathbf{L_2}$ direction with finite N_y.

In a tight-binding model in terms of p_z atomic orbitals, the Hamiltonian of tBLGNRs in the Majorana physics regime is written as

$$H = -\sum_{i,j,\sigma} t(\mathbf{r}_i - \mathbf{r}_j) c^+_{i\sigma} c_{j\sigma} + i\lambda \sum_{i,j,\sigma,\sigma'} c^+_{i,\sigma} (\widehat{\boldsymbol{\delta}} \times \boldsymbol{\sigma})_z^{\sigma\sigma'} c_{j,\sigma'} + V_Z \sum_{i,\sigma,\sigma'} c^+_{i,\sigma} \sigma_\alpha^{\sigma\sigma'} c_{i,\sigma'} + \Delta \sum_i c^+_{i,\uparrow} c^+_{i,\downarrow} + \text{H.c.}, \quad (2)$$

where $c^+_{i\sigma}$ creates an electron with spin σ at site i of the honeycomb lattice and $\widehat{\boldsymbol{\delta}} = \boldsymbol{\delta}/a_0$ is a unit vector with $\boldsymbol{\delta}$ the vectors in Fig. 1(a) and a_0 for the carbon-carbon distance. The first term in Eq. (2) is bilayer graphene's tight-binding Hamiltonian. The second term is the Rashba SOC with strength λ. The third term is the Zeeman coupling, and the last term is the induced s-wave superconductivity [40]. $t(\mathbf{r}_i - \mathbf{r}_j)$ is the transfer integral between site i and site j, and the following approximation is adopted [27,47–51]:

$$-t(\mathbf{d}) = V_{pp\pi}\left[1 - \left(\frac{\mathbf{d}\cdot\mathbf{e}_z}{d}\right)^2\right] + V_{pp\sigma}\left(\frac{\mathbf{d}\cdot\mathbf{e}_z}{d}\right)^2,$$
$$V_{pp\pi} = V^0_{pp\pi} \exp\left(-\frac{d-a_0}{\delta_0}\right),$$
$$V_{pp\sigma} = V^0_{pp\sigma} \exp\left(-\frac{d-d_0}{\delta_0}\right), \quad (3)$$

where $\mathbf{d} = \mathbf{r}_i - \mathbf{r}_j$, and $\mathbf{e}_z$ is the unit vector parallel to the z axis. $V^0_{pp\pi}$ is the transfer integral between the nearest-neighbor atoms of monolayer graphene, which are located at a carbon-carbon distance $a_0 \approx 0.142$ nm, and $V^0_{pp\sigma}$ is the interlayer transfer integral between vertically located atoms at the interlayer distance $d_0 \approx 0.335$ nm. We take $V^0_{pp\pi} \approx -2.7$ eV and $V^0_{pp\sigma} \approx 0.48$ eV to fit the dispersions of monolayer graphene and AB-stacked bilayer graphene. δ_0 is the decay length of the transfer integral, and is chosen as $0.184a$ ($a = \sqrt{3}a_0$) so that the next-nearest intralayer coupling becomes $0.1V^0_{pp\pi}$ [27,51]. t_0 represents the nearest intralayer coupling, and $|t_0| = 2.7$ eV is as the energy unit throughout the paper. The transfer integral for $d > 4a_0$ is exponentially small and can be safely neglected.

According to the symmetry classification of topological systems this model belongs to Bogoliubov–de Gennes class D [52], as the Zeeman term breaks the time-reversal symmetry. The topology of this class in one dimension can be characterized by a Z_2 number, which is associated with the Berry phase [46,53]. In our system, we calculate the Berry phase γ for the lower half bands to discriminate between topologically trivial and nontrivial phases, where $\gamma = \pi$ in the topological nontrivial phase and $\gamma = 0$ in the trivial phase. The topological phase transition can also be identified by the presence of a finite gap with a gap closing point separating the two phases. For a fully open system, such as finite length ribbons, the presence of zero-energy states and the Majorana polarization are two evidences to verify the Majorana bound states.

The Majorana polarization (MP) is defined as follows [54–59]. A Majorana state is an eigenstate of the particle-hole operator. Therefore, a Majorana-like state localized inside a spatial region R must satisfy $C = 1$, where C is the magnitude of the integral of the Majorana polarization vector over the spatial region R:

$$C = \frac{|\sum_{j\in R}\langle\Psi|C_j|\Psi\rangle|}{\sum_{j\in R}\langle\Psi|\widehat{r}_j|\Psi\rangle}, \quad (4)$$

where $\widehat{r}_j$ is the projection onto site j and $C_j \equiv C\widehat{r}_j$. The local MP is simply the expectation value of the local particle-hole transformation:

$$\langle\Psi|C_j|\Psi\rangle = -2\sum_\sigma \sigma \mu_{j\sigma}\nu_{j\sigma}. \quad (5)$$

In the Nambu basis, an eigenstate j of the tight-binding Hamiltonian can be written as $\Psi_j^T = (\mu_{j\uparrow}, \mu_{j\downarrow}, \nu_{j\downarrow}, \nu_{j\uparrow})$, where μ and ν denote the electron and hole components, respectively. In general we take R to correspond to half of the system, divided usually along the longer length. Meanwhile, for a Majorana state, the local structure of the MP defined in Eq. (5) needs to be aligned inside R ("ferromagnetic" MP structure).

For the tBLGNRs, the low-energy electronic structures are closely related to the spatially inhomogeneous interlayer coupling. Thus, the topological superconductivity can be adjusted by changing the spatially inhomogeneous character, which mainly depends on two key parameters: the twist angle and the interlayer coupling. In this work, the twist angle is fixed equal to $\varphi = 21.8°$, while the interlayer coupling is redistributed by two methods: the parallel interlayer dislocation d_s and uniaxial strain $\boldsymbol{\epsilon}$. For the interlayer dislocation, without loss of generality, we move the two layers of tBLGNR in opposite directions along $\mathbf{L_2}$ and define the ratio of relative displacement as $d_s = \Delta y/L_2$, where Δy is the relative displacement between the two layers. For the second method, the tension $\mathbf{T}$ is applied. When stress is induced in graphene by mechanical action on the substrate, the relevant parameter is in fact the tensile strain $\boldsymbol{\epsilon}$, rather than the tension $\mathbf{T}$. For this reason, we treat $\boldsymbol{\epsilon}$ as the tunable parameter. The tensor strain in the lattice coordinate system reads [40,60]

$$\boldsymbol{\epsilon} = \varepsilon\begin{pmatrix} \cos^2\theta - \sigma\sin^2\theta & (1+\sigma)\cos\theta\sin\theta \\ (1+\sigma)\cos\theta\sin\theta & \sin^2\theta - \sigma\cos^2\theta \end{pmatrix}, \quad (6)$$

where ε is the strength of tensile strain, and σ is the Poisson ratio for graphene, $\sigma = 0.165$. θ is the angle between the strain $\boldsymbol{\epsilon}$ and the zigzag direction [shown in Fig. 1(a)]. The deformed vector is given to leading order by the transformation

$$\boldsymbol{\nu} = (1 + \boldsymbol{\epsilon})\cdot\boldsymbol{\nu}^0, \quad (7)$$

where $\boldsymbol{\nu}^0$ represents a general vector in the undeformed graphene plane.

III. MAJORANA ZERO MODES AND THE TOPOLOGICAL INVARIANTS

We consider an infinite ribbon with open boundary conditions in the $\mathbf{L_2}$ direction ($N_y = 6$) and set $k \equiv k_{L_1}$ in the following discussion. The inhomogeneous interlayer coupling breaks the lattice symmetry at the edge and induces two nonequivalent edges [32,33,44], called edge 1 and edge 2,

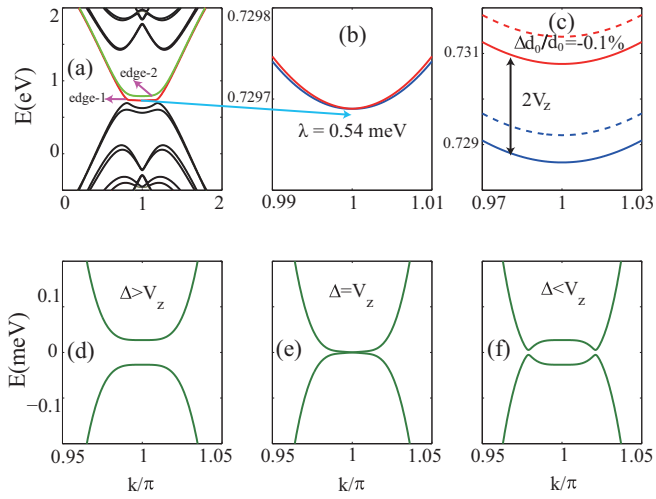

FIG. 2. The lowest energy band for (1,2) tBLGNRs with $N_y = 6$. (a) Split edge states due to inhomogeneous interlayer coupling. State 1 localizes at edge 1 with the stronger interlayer coupling, and state 2 localizes at edge 2 with the weaker interlayer coupling. (b) Rashba SOC induced spin split of state 1 with $\lambda = 0.54$ meV and (c) spin-resolved band shift due to Zeeman coupling with spin gap equal to $2V_Z$ ($V_Z = 1.08$ meV). Solid curves, bands with interlayer distance $d_0 = 0.335$ nm; dashed curves, bands with a little smaller interlayer distance. (d–f) Topological trivial to nontrivial evolution of superconducting gap versus Δ and V_Z.

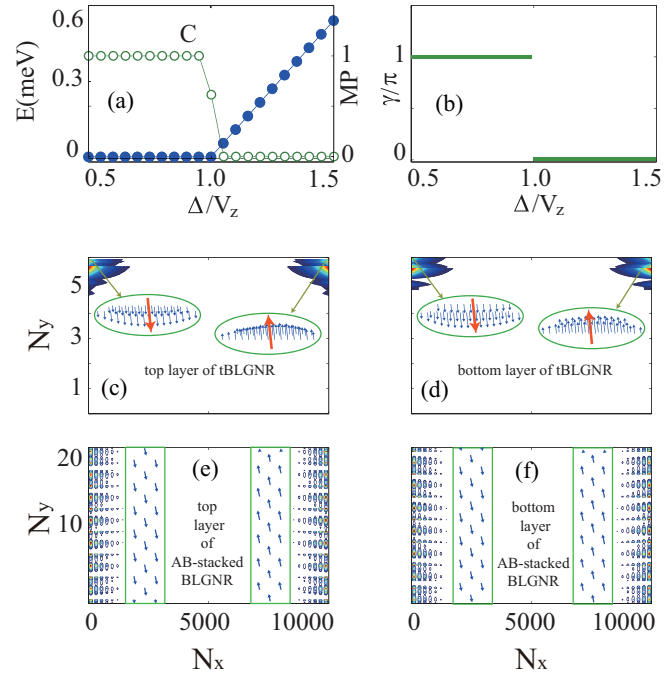

FIG. 3. Majorana zero modes and topological invariants. (a) Energy eigenvalues (blue curve, solid circles) closest to zero and MP C (green curve, open circles) as a function of Δ/V_Z for a quasi-1D (1,2) tBLGNR with $N_x = 10\,000$ and $N_y = 6$. (b) Berry phase γ versus Δ/V_Z for a periodic (1,2) tBLGNR with $N_y = 6$. (c, d) Real-space distribution of the MZMs in top layer and bottom layer of quasi-1D (1,2) tBLGNRs. The quasi-1D topological superconductivity is achieved at edge 1, and the MZMs localize at both ends of edge 1. (e, f) Real-space distribution of the MZMs in a finite *AB*-stacked armchair GNR with $N_x = 10\,000$ and $N_y = 21$ eight-atom unit cells. The arrows in (c–f) represent local MP at partial carbon atoms for the zero-energy states.

as shown in Fig. 1(b). Correspondingly, the band structure shows two separate edge states [Fig. 2(a)], called state 1 and state 2. The upper-energy state (state 2) favors to localize at edge 2 which has the weaker interlayer coupling, while the lower-energy state (state 1) favors to localize at edge 1 which has the stronger interlayer coupling. The lower-energy edge state (state 1) is stable, and we focus on the lower-energy state hereafter. In Fig. 2(b), the Rashba SOC lifts the spin degeneracy of state 1 by displacing the parabolic bands horizontally in opposite directions. The Zeeman coupling lifts the remaining spin degeneracy at $kL_1 = \pi$, opening up a gap of value $2V_Z$ as shown in Fig. 2(c). As described below, the two spin-split edge states can be shifted up overall by decreasing the interlayer distance of tBLGNR, as indicated by the dashed curves in Fig. 2(c). If the chemical potential is inside the gap shown in Fig. 2(c), a finite s-wave superconducting pairing can induce 1D topological superconductivity on the corresponding edge. The system becomes gapped as shown in Fig. 2(d) for $\Delta > V_Z$, goes through a gapless transition point at $\Delta = V_Z$ [Fig. 2(e)], and becomes gapped again for $\Delta < V_Z$ [Fig. 2(f)].

In order to determine whether this is a topological transition, we have computed the low-energy spectrum and the MP C for a ribbon of finite length, Fig. 3(a), as well as the Berry phase γ for infinite ribbon, Fig. 3(b). It is clearly shown that a finite Berry phase $\gamma = \pi$ in Fig. 3(b) correlates with the presence of zero-energy Majorana modes and $C = 1$ in Fig. 3(a) for $\Delta < V_Z$. The transition to the trivial phase is signaled in Fig. 3(a) by the absence of $C = 1$ and zero-energy Majorana modes, and in Fig. 3(b) by a zero Berry phase $\gamma = 0$. In Fig. 3(a) we use a finite-size system bounded in the $\mathbf{L_1}$ direction ($N_x = 10\,000$ and $N_y = 6$), while in Fig. 3(b) periodic boundary conditions along $\mathbf{L_1}$ are used (keeping $N_y = 6$).

It is well established that in a 1D topological superconductor the Majorana fermions appear as end states in real space. Figures 3(c) and 3(d) show the real-space distribution of the Majorana zero mode wave function on top and bottom layers of tBLGNRs. It is clearly seen that the edge supports robust topological Majorana bound states at the edge ends. To further verify the existence of Majorana zero modes in the fully open ribbons, the local Majorana polarization is calculated, shown in the green ellipses in Figs. 3(c) and 3(d). We can see the formation of two "ferromagnetic" states localized at the two ends of the edge, with opposite MP. The zero-energy states also satisfy $C = 1$, which is both a necessary and sufficient condition for a state being a Majorana state. The quasi-1D real-space distribution of MZMs of the tBLGNR is obviously different from that of untwisted bilayer graphene nanoribbons (BLGNRs). For comparison, the Majorana zero modes in *AB*-stacked BLGNRs are calculated [Figs. 3(e)–3(f)], which satisfy $C = 1$ and present "ferromagnetic" MP structure. Because the interlayer coupling is uniform in the *AB*-stacked BLGNR with armchair edges, the two ribbon edges are equivalent. Therefore, the Majorana zero modes

localize at the two narrow ribbon ends, whose topological behaviors are the same as for a single-layer armchair ribbon [40].

IV. RESULTS AND DISCUSSION

A. The "jump" of Majorana zero modes between 1D ribbon edges

As discussed above, the topological invariants in an infinite tBLGNR and the MP in the quasi-1D ribbons ($N_x \gg N_y$) give the same phase diagram. In this section, we discuss the 1D topological superconductivity at the edge of quasi-1D tBLGNRs. It is known that the inhomogeneous interlayer coupling splits the edge states in energy, and the lower-energy state favors to localize at the edge with stronger interlayer coupling. By introducing the interlayer dislocation d_s and uniaxial strain ε, the strength of interlayer coupling at edge 1 may be reduced lower than that at edge 2, corresponding with the exchange of position of state 1 and state 2. As shown in Fig. 4, when d_s and/or ε increase above the critical values, the lower-energy edge changes from edge 1 to edge 2, and the 1D topological superconductivity appears at edge 2. More importantly, the dislocation- [Figs. 4(a) and 4(b)] and strain-induced [Figs. 4(c) and 4(d)] MZM transfer between edge 1 and edge 2 occurs immediately without the process along the ribbon end, just like a "jump" behavior.

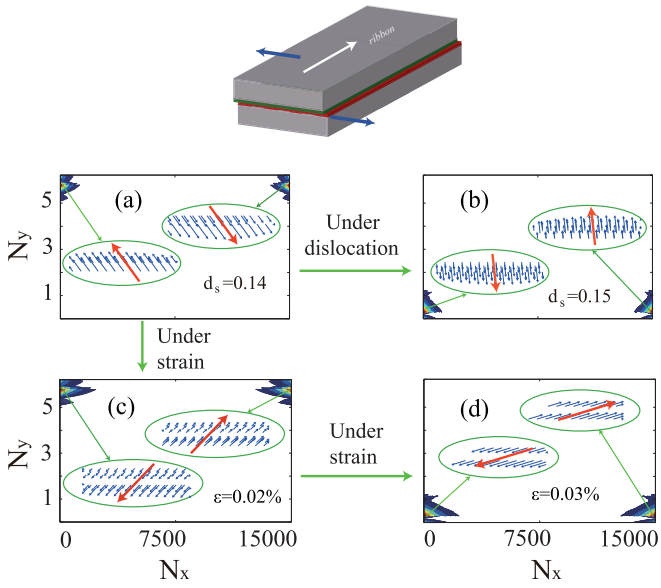

FIG. 4. The 1D topological superconductivity and Majorana end states "jump" from one edge of (1,2) tBLGNRs to the opposite edge, induced by the (a, b) interlayer dislocation and (c, d) uniaxial strain. In (a) and (c), dislocation and strain are below the critical values, and in (b) and (d) they are above. With the increase of d_s and/or ε, the lower-energy edge state changes and the 1D topological superconductivity appears at opposite edges. The "ferromagnetic" MP structures in the ellipses confirm the existence of Majorana states in a quasi-1D system. The used parameters are the same as in Fig. 2; the finite tBLGNR size is $N_y = 6$ and $N_x = 1.5 \times 10^4$.

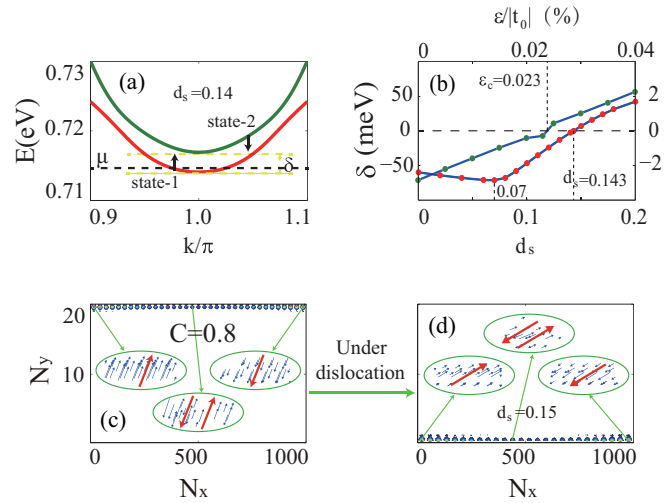

FIG. 5. (a, b) The evolution of the two edge states as function of interlayer dislocation d_s and uniaxial strain ε. At the critical values, $d_s = 0.143$ and $\varepsilon/|t_0| = 0.023\%$, the two edge states cross at $k = \pi$ and the lower-energy edge changes beyond the critical values. The chemical potential μ (black dashed line) is fixed in the topological region of the lower-energy edge state. (c, d) The jump behaviors between edge 1 and edge 2 in a wider ribbon. The local MP shows that the two "quasi-Majorana" end states overlap with each other in the middle of the edge.

The mechanism of the jump behaviors can be understood from the evolution of the two edge states of infinite tBLGNRs with periodic boundary conditions. When the chemical potential is fixed in the topological region of the lower-energy edge state, such an edge will be in a topological nontrivial phase. Under the dislocation, the bottom layer of tBLGNR moves to the $-\mathbf{L_2}$ direction and the top layer moves to the $\mathbf{L_2}$ direction, and the strength of the interlayer coupling at the two edges is tuned. In the band structure, a relative movement occurs between the energy of the two edges, as shown in Fig. 5(a). We define a gap $\delta = E_1 - E_2$ to describe the energy difference between state 1 and state 2. The blue curve with red dots in Fig. 5(b) presents the evolution of the gap between two edge states as a function of dislocation d_s. For small d_s, both state 1 and state 2 move to the lower energy simultaneously. State 1 moves faster, so the absolute values of δ increase first. When $d_s \gtrsim 0.07$, state 1 reverses to higher energy, while state 2 goes on to lower energy. Until at the critical value of $d_s = 0.143$, the two edge states cross and δ is roughly equal to zero. Above the critical value, the two edge states split again. Edge 1 moves to higher energy and edge 2 moves to lower energy, so δ is positive. Similar behavior can be found when a uniaxial strain ε is supplied, because it changes the atom coordinate so as to redistribute the strength of interlayer coupling at the edges of the moiré superlattice. The blue curve with green dots in Fig. 5(b) presents the evolution of the δ as a function of uniaxial strain ε. With the increase of ε, δ increases from negative values to positive values, which indicates the exchange of the two edge states and the "jump" of MZMs from edge 1 to edge 2 at $\varepsilon = 0.023\%$. Note that the jumplike behaviors can be observed by fine-tuning the parameters and proper operations. It is helpful to reveal the

connection between inhomogeneous interlayer coupling and the low-energy edge state property in a twisted bilayer system.

In order to verify the universality of the "jump" behaviors in tBLGNRs under dislocation and uniaxial strain, a wider and shorter tBLGNR ($N_y = 20$ and $N_x = 1000$) is investigated as shown in Figs. 5(c) and 5(d). The parameters used are in the topological nontrivial region of infinite tBLGNR with periodic boundary conditions along $\mathbf{L_1}$. We can find that one 1D state still localizes at one of the longer edges, which acts like a topological wire. As the length and the width become comparable, the in-gap states have nonzero but very small energies, which are called "quasi-Majorana" states [55,56,59]. The entire topological phase is characterized now by $C \approx 0.8$. Two "ferromagnetic" states with opposite MP at the edge ends overlap in the middle of this edge, which is clearly seen from the local structure of the MP. For such a wider and shorter tBLGNR, we can still see the jump behaviors of the quasi-Majorana states induced by the interlayer dislocation [Fig. 5(d)]. If $N_x \gg N_y$ ($N_y = 20$ and $N_x = 5000$), the quasi-Majorana states can become Majorana states, and the topological behaviors are the same as in the narrow case ($N_y = 6$ and $N_x = 10\,000$). The topological superconductivity in (4,5) tBLGNRs is also investigated, and similar topological "jump" behaviors are obtained.

B. Transferring a Majorana zero mode along the 1D ribbon edge

Comparing to other platforms, the advantage of MZMs in tBLGNRs lies in their rich tunability and good controllability. By applying gate voltage bias between the bilayers ($\Delta\mu$) or changing the interlayer distance (Δd_0), the MZM can be transferred along the 1D ribbon edge, as shown in Fig. 6. The 1D topological superconductivity can be supported by one edge of (1,2) tBLGNR, and the MZMs localize at two ends of this edge. When the gate bias or interlayer distance are above the critical values of the topological nontrivial phase, i.e., $\Delta\mu > \Delta\mu_c$ and/or $\Delta d_0 > \Delta d_{0c}$, the topological phase transition occurs and the related region enters into the trivial phase. The topological invariant γ for infinite tBLGNR and the MP C for finite tBLGNR are checked as a function of $\Delta\mu$ [Fig. 6(b)] and Δd_0 [Fig. 6(e)]. In this case, the MZMs are driven to transfer along the ribbon edge by voltage bias [Fig. 6(c)] and stress [Fig. 6(f)].

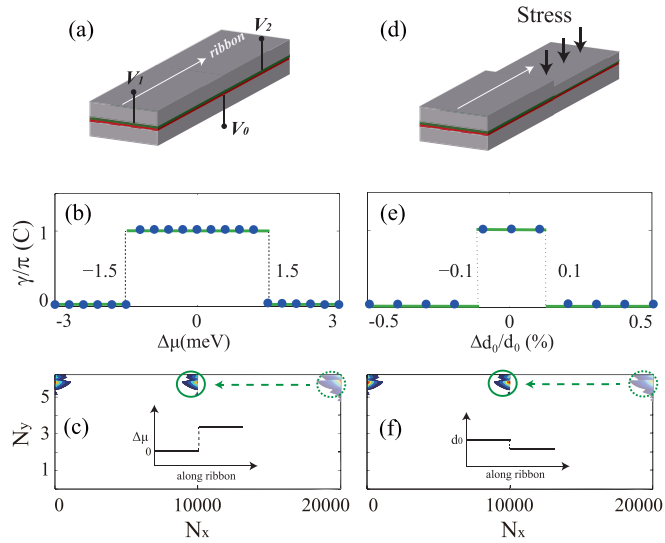

FIG. 6. The transfer of a MZM along the stronger interlayer coupling edge of (1,2) tBLGNR as a function of (a–c) gate voltage bias $\Delta\mu$ and (d–f) interlayer distance d_0. (a) Three gates are used to control the chemical potential of related regions. The chemical potential of the bottom layer is fixed by gate V_0, and the chemical potentials of the two ends of the top layer are controlled by gates V_1 and V_2, respectively. (b) Berry phase (green lines) for the infinite ribbon and the MP C (blue dots) for the fully open ribbon are given as a function of $\Delta\mu$. The same phase diagram is obtained. Above the critical value, the related region enters into a trivial phase and the MZMs are transferred, as shown in (c). (d–f) The interlayer distance can be decreased by pressure and, therefore, transfer a MZM. The used parameters are the same as in Fig. 2.

V. EXPERIMENTAL REALIZATION

In order to realize Majorana zero modes in tBLGNRs using the standard scheme and then manipulate them through interlayer dislocation, strain, gate bias, and interlayer distance, a sizable superconducting gap, Zeeman field, and Rashba SOC are required and needed. We show here that such requirements are within experimental reach.

Twisted bilayer nanoribbons have been obtained by unzipping chiral multiwalled nanotubes [61]. Sandwiched between the high-SOC transition-metal dichalcogenide WS_2 [34,62,63] and ferromagnetic insulator EuS [64], the SOC in bilayer GNRs can be enhanced by several orders, and the Zeeman field can achieve values comparable to those in Rashba nanowires. By decorating monolayer graphene with the alkali-metal atoms Ca [65] and Li [66], or fabricating Ca-intercalated bilayer graphene [67], a superconducting gap of $\Delta \sim 1$ meV has been shown. Three gates on BLGNRs are used to control the chemical potential of each layer. To make the interlayer distance have higher tunability, each layer of the bilayer ribbon is deposited on WS_2 and EuS substrates, respectively. The interlayer variation can be tuned by moving the substrate. In Ref. [37], a spatially varying magnetic field was shown to give rise to an additional term in the Hamiltonian which is equivalent to SOC, thus mitigating the lack of SOC in graphene.

VI. CONCLUSIONS

In conclusion, we propose a platform, twisted bilayer graphene nanoribbons, to realize and regulate 1D topological superconductivity and Majorana zero modes in the presence of Rashba spin-orbit coupling, Zeeman field, and s-wave superconductivity. Due to the spatially inhomogeneous interlayer coupling between bilayers, two edge states are split in energy. When the chemical potential is fixed at the lower-energy edge state, the system is in the topological region, which can be confirmed by evaluating the Berry phase and Majorana polarization of an infinite and a finite ribbon, respectively. Simultaneously, the ribbon edge with stronger interlayer coupling will be in a topological nontrivial phase and acts as a 1D topological wire. Majorana zero modes localize

at both ends of this edge. By changing the interlayer dislocation and introducing the uniaxial strain, the strength of the interlayer coupling at both edges can be redistributed. Upon the critical values, the positions of two edge states exchange in energy, and the 1D topological superconductor "jumps" to the other edge. Moreover, the Majorana zero modes localized at both ends of a 1D topological superconductor edge can be tuned to transfer along this ribbon edge by gate voltage bias between the bilayers and interlayer distance.

ACKNOWLEDGMENTS

The authors express their gratitude to Dong-Hui Xu for many helpful discussions. This work was supported by the National Key Research and Development Program of China (Grant No. 2016YFA0300300) and the National Natural Science Foundation of China (Grants No. 11904234, No. 11774238, No. 11674151, No. 11604138, No. 11874234, and No. 11574220).

[1] V. Mourik, K. Zuo, S. M. Frolov, S. Plissard, E. Bakkers, and L. P. Kouwenhoven, Science **336**, 1003 (2012).

[2] M. Deng, C. Yu, G. Huang, M. Larsson, P. Caroff, and H. Xu, Nano Lett. **12**, 6414 (2012).

[3] A. Das, Y. Ronen, Y. Most, Y. Oreg, M. Heiblum, and H. Shtrikman, Nat. Phys. **8**, 887 (2012).

[4] L. P. Rokhinson, X. Liu, and J. K. Furdyna, Nat. Phys. **8**, 795 (2012).

[5] A. D. K. Finck, D. J. Van Harlingen, P. K. Mohseni, K. Jung, and X. Li, Phys. Rev. Lett. **110**, 126406 (2013).

[6] S. M. Albrecht, A. Higginbotham, M. Madsen, F. Kuemmeth, T. S. Jespersen, J. Nygård, P. Krogstrup, and C. Marcus, Nature (London) **531**, 206 (2016).

[7] S. Nadj-Perge, I. K. Drozdov, J. Li, H. Chen, S. Jeon, J. Seo, A. H. MacDonald, B. A. Bernevig, and A. Yazdani, Science **346**, 602 (2014).

[8] Q. L. He, L. Pan, A. L. Stern, E. C. Burks, X. Che, G. Yin, J. Wang, B. Lian, Q. Zhou, E. S. Choi *et al.*, Science **357**, 294 (2017).

[9] D. A. Ivanov, Phys. Rev. Lett. **86**, 268 (2001).

[10] M. Leijnse and K. Flensberg, Semicond. Sci. Technol. **27**, 124003 (2012).

[11] C. Nayak, S. H. Simon, A. Stern, M. Freedman, and S. Das Sarma, Rev. Mod. Phys. **80**, 1083 (2008).

[12] S. D. Sarma, M. Freedman, and C. Nayak, npj Quantum Inf. **1**, 15001 (2015).

[13] J. M. B. Lopes dos Santos, N. M. R. Peres, and A. H. Castro Neto, Phys. Rev. Lett. **99**, 256802 (2007).

[14] R. Bistritzer and A. H. MacDonald, Proc. Natl. Acad. Sci. USA **108**, 12233 (2011).

[15] E. J. Mele, Phys. Rev. B **81**, 161405(R) (2010).

[16] M. Koshino, N. F. Q. Yuan, T. Koretsune, M. Ochi, K. Kuroki, and L. Fu, Phys. Rev. X **8**, 031087 (2018).

[17] H. C. Po, L. Zou, A. Vishwanath, and T. Senthil, Phys. Rev. X **8**, 031089 (2018).

[18] J.-B. Qiao, L.-J. Yin, and L. He, Phys. Rev. B **98**, 235402 (2018).

[19] X. Lu, P. Stepanov, W. Yang, M. Xie, M. A. Aamir, I. Das, C. Urgell, K. Watanabe, T. Taniguchi, G. Zhang *et al.*, arXiv:1903.06513.

[20] Y. Cao, D. Rodan-Legrain, O. Rubies-Bigordà, J. M. Park, K. Watanabe, T. Taniguchi, and P. Jarillo-Herrero, arXiv:1903.08596.

[21] Y. Zhang, T.-T. Tang, C. Girit, Z. Hao, M. C. Martin, A. Zettl, M. F. Crommie, Y. R. Shen, and F. Wang, Nature (London) **459**, 820 (2009).

[22] E. V. Castro, K. S. Novoselov, S. V. Morozov, N. M. R. Peres, J. M. B. Lopes dos Santos, J. Nilsson, F. Guinea, A. K. Geim, and A. H. Castro Neto, Phys. Rev. Lett. **99**, 216802 (2007).

[23] P. Tan, W. Han, W. Zhao, Z. Wu, K. Chang, H. Wang, Y. Wang, N. Bonini, N. Marzari, N. Pugno *et al.*, Nat. Mater. **11**, 294 (2012).

[24] A. C. Ferrari, J. C. Meyer, V. Scardaci, C. Casiraghi, M. Lazzeri, F. Mauri, S. Piscanec, D. Jiang, K. S. Novoselov, S. Roth *et al.*, Phys. Rev. Lett. **97**, 187401 (2006).

[25] F. Wang, Y. Zhang, C. Tian, C. Girit, A. Zettl, M. Crommie, and Y. R. Shen, Science **320**, 206 (2008).

[26] K. F. Mak, C. H. Lui, J. Shan, and T. F. Heinz, Phys. Rev. Lett. **102**, 256405 (2009).

[27] G. Trambly de Laissardiere, D. Mayou, and L. Magaud, Nano Lett. **10**, 804 (2010).

[28] G. Trambly de Laissardière, D. Mayou, and L. Magaud, Phys. Rev. B **86**, 125413 (2012).

[29] Y. Cao, V. Fatemi, A. Demir, S. Fang, S. L. Tomarken, J. Y. Luo, J. D. Sanchez-Yamagishi, K. Watanabe, T. Taniguchi, E. Kaxiras *et al.*, Nature (London) **556**, 80 (2018).

[30] Y. Cao, V. Fatemi, S. Fang, K. Watanabe, T. Taniguchi, E. Kaxiras, and P. Jarillo-Herrero, Nature (London) **556**, 43 (2018).

[31] M. Yankowitz, S. Chen, H. Polshyn, Y. Zhang, K. Watanabe, T. Taniguchi, D. Graf, A. F. Young, and C. R. Dean, Science **363**, 1059 (2019).

[32] E. Suárez Morell, R. Vergara, M. Pacheco, L. Brey, and L. Chico, Phys. Rev. B **89**, 205405 (2014).

[33] M. Pelc, E. S. Morell, L. Brey, and L. Chico, J. Phys. Chem. C **119**, 10076 (2015).

[34] A. Avsar, J. Y. Tan, T. Taychatanapat, J. Balakrishnan, G. Koon, Y. Yeo, J. Lahiri, A. Carvalho, A. Rodin, E. O'Farrell *et al.*, Nat. Commun. **5**, 4875 (2014).

[35] Z. Wang, D.-K. Ki, J. Y. Khoo, D. Mauro, H. Berger, L. S. Levitov, and A. F. Morpurgo, Phys. Rev. X **6**, 041020 (2016).

[36] J. Balakrishnan, G. Kok Wai Koon, M. Jaiswal, A. H. Castro Neto, and B. Özyilmaz, Nat. Phys. **9**, 284 (2013).

[37] J. Klinovaja and D. Loss, Phys. Rev. X **3**, 011008 (2013).

[38] C. Dutreix, C. Bena, M. Guigou, and D. Chevallier, Eur. Phys. J. **87**, 296 (2013).

[39] C. Chamon, C.-Y. Hou, C. Mudry, S. Ryu, and L. Santos, Phys. Scr. **2012**, 014013 (2012).

[40] Z.-H. Wang, E. V. Castro, and H.-Q. Lin, Phys. Rev. B **97**, 041414(R) (2018).

[41] P. San-Jose, J. L. Lado, R. Aguado, F. Guinea, and J. Fernández-Rossier, Phys. Rev. X **5**, 041042 (2015).

[42] O. Gröning, S. Wang, X. Yao, C. A. Pignedoli, G. Borin Barin, C. Daniels, A. Cupo, V. Meunier, X. Feng, A. Narita *et al.*, Nature (London) **560**, 209 (2018).
[43] A. M. Alsharari, M. M. Asmar, and S. E. Ulloa, Phys. Rev. B **97**, 241104(R) (2018).
[44] R.-L. Chu, G.-B. Liu, W. Yao, X. Xu, D. Xiao, and C. Zhang, Phys. Rev. B **89**, 155317 (2014).
[45] G. Xu, J. Wang, B. Yan, and X.-L. Qi, Phys. Rev. B **90**, 100505(R) (2014).
[46] L. Li, E. V. Castro, and P. D. Sacramento, Phys. Rev. B **94**, 195419 (2016).
[47] P. Moon and M. Koshino, Phys. Rev. B **85**, 195458 (2012).
[48] P. Moon and M. Koshino, Phys. Rev. B **87**, 205404 (2013).
[49] J. C. Slater and G. F. Koster, Phys. Rev. **94**, 1498 (1954).
[50] T. Nakanishi and T. Ando, J. Phys. Soc. Jpn. **70**, 1647 (2001).
[51] S. Uryu, Phys. Rev. B **69**, 075402 (2004).
[52] A. P. Schnyder, S. Ryu, A. Furusaki, and A. W. W. Ludwig, Phys. Rev. B **78**, 195125 (2008).
[53] J. C. Budich and E. Ardonne, Phys. Rev. B **88**, 075419 (2013).
[54] V. Kaladzhyan and C. Bena, SciPost Phys. **3**, 002 (2017).
[55] N. Sedlmayr and C. Bena, Phys. Rev. B **92**, 115115 (2015).
[56] N. Sedlmayr, J. M. Aguiar-Hualde, and C. Bena, Phys. Rev. B **93**, 155425 (2016).
[57] D. Sticlet, C. Bena, and P. Simon, Phys. Rev. Lett. **108**, 096802 (2012).
[58] V. Kaladzhyan, J. Despres, I. Mandal, and C. Bena, Eur. Phys. J. B **90**, 211 (2017).
[59] N. Sedlmayr, V. Kaladzhyan, C. Dutreix, and C. Bena, Phys. Rev. B **96**, 184516 (2017).
[60] V. M. Pereira, A. H. Castro Neto, and N. M. R. Peres, Phys. Rev. B **80**, 045401 (2009).
[61] L. Xie, H. Wang, C. Jin, X. Wang, L. Jiao, K. Suenaga, and H. Dai, J. Am. Chem. Soc. **133**, 10394 (2011).
[62] Z. Wang, D.-k. Ki, H. Chen, H. Berger, A. H. MacDonald, and A. F. Morpurgo, Nat. Commun. **6**, 8339 (2015).
[63] B. Yang, M.-F. Tu, J. Kim, Y. Wu, H. Wang, J. Alicea, R. Wu, M. Bockrath, and J. Shi, 2D Mater. **3**, 031012 (2016).
[64] P. Wei, S. Lee, F. Lemaitre, L. Pinel, D. Cutaia, W. Cha, F. Katmis, Y. Zhu, D. Heiman, J. Hone *et al.*, Nat. Mater. **15**, 711 (2016).
[65] J. Chapman, Y. Su, C. Howard, D. Kundys, A. Grigorenko, F. Guinea, A. Geim, I. Grigorieva, and R. Nair, Sci. Rep. **6**, 23254 (2016).
[66] B. Ludbrook, G. Levy, P. Nigge, M. Zonno, M. Schneider, D. Dvorak, C. Veenstra, S. Zhdanovich, D. Wong, P. Dosanjh *et al.*, Proc. Natl. Acad. Sci. USA **112**, 11795 (2015).
[67] S. Ichinokura, K. Sugawara, A. Takayama, T. Takahashi, and S. Hasegawa, ACS Nano **10**, 2761 (2016).